Numerical Simulation of Condensate Layer Formation During Vapour Phase Soldering

Balázs Illés, Attila Géczy

Department of Electronics Technology, Budapest University of Technology and Economics,

Egry József str. 18, H-1111 Budapest, Hungary

billes@ett.bme.hu

Abstract: This paper presents a modeling approach of the condensate layer formation on the surface of printed circuit boards during Vapour Phase Soldering (VPS) process. The condensate layer formation model is an extension to a previously developed board level condensation model, which calculates the mass of the condensed material on the surface of the soldered printed circuit board. The condensate layer formation model applies combined transport mechanisms including convective mass transport due to the hydrostatic pressure difference in the layer and the gravity force; conductive and convective energy transport. The model can describe the dynamic formation and change of the condensate layer after the immersion of the soldered assembly into the saturated vapour space and can calculate the mass and energy transport in the formed condensate layer. This way the effect of the condensate layer changes on the heating of the soldered assembly can be investigated. It was shown that the numerical modeling of the VPS process becomes more accurate with application of dynamic condensate layer instead of a static description.

Keywords: Vapour phase soldering, Condensate layer, Galden, Heat transfer, Reflow soldering

Nomenclature		A surface, m^2
		σ surface tension, N/m
v	velocity, m/s	θ decline angle of the board, rad
ρ	density, kg/m^3	n indexing of the mesh
P_h	hydrostatic pressure, Pa	$\Delta x, \Delta y, \Delta z$ resolution of the mesh, mm
g	gravity acceleration, m/s^2	$\bar{r}$ local vector
t	time, s	Δt time step, s
T	temperature, K	
q_m	mass flow, kg/s	**Abreviations:**
υ	kinematic viscosity, $\text{m}^2\text{/s}$	l liquid
λ	specific thermal cond., W/m.K	v vapour
C_S	specific heat capacity, J/kg.K	f flowing
h	height of condensate, m	d dropping

1. Introduction

 The Vapour Phase Soldering (VPS) or condensation soldering is an emerging reflow soldering technology in electronics industry, which could be a future alternative of forced convection and infrared reflow methods. During the VPS process a special heat transfer liquid (called Galden^{TM}) is boiled in a closed tank until a saturated vapour space is generated. After the saturation the prepared assembly is immersed into the vapour space, the vapour condenses and forms a continuous condensate layer on the surface of the assembly. The condensate layer – which heats the assembly above the melting point of the applied solder alloy – is heated by the latent heat of condensation and the heat from the surrounding medium (vapour). The Galden liquid [1] is composed of perfluoropolyether substance (PFPE):

$$CF_3 - (OCFCF_2)_n - (OCF_2)_m - OCF_3$$
$$|$$
$$CF_3$$

(1)

where the flexible ether chain structure is closed with strong carbon-fluorine bonds providing stability. Galden liquid is produced with various boiling points (from 150ºC up to 240ºC) fitting the melting point of the applied solder alloy.

 The condensation heating or cooling is a widely applied technology due to its high efficiency which makes this technology suitable for heating of facilities via heat pumps [2] and for cooling of electronics appliances via heat pipes [3]. In addition, the condensation plays an important role not only in direct condensational applications but in other various applications, such as the ventilation pipes of deeply buried tunnels [4] or in the technologies of CO_2 separation from steam [5]. From the point of soldering technology the most important advantages of VPS method are the almost uniform heating and the elimination of overheating since the maximum temperature during the soldering is equal with the boiling point of the applied heat transfer liquid [6, 7]. Vapour phase soldering also eliminates the shadowing effect in the case of small size components what is a frequent problem during the forced convection reflow soldering. During the VPS process oxidation of the solder joints is also avoided due to the inert atmosphere in the VPS tank and the condensate film layer on the assembly [8].

 Without proper control, the major disadvantage of the VPS process is the high heating gradient, while the heat transfer coefficient of the vapour can be much higher than in a forced convection oven [9]. This can result in soldering failures such as tombstoning, solder cracking, solder beading [10], solder voiding [11]; popcorn cracks of the packages and delamination of packages and PCBs [12]. Nowadays, there are a lot of technical innovations to reduce the

previously mentioned soldering failures such as application of vacuum atmosphere [13] and soft vapour technology [14]. There are also some examples for the characterization of the VPS process parameters (concentration and temperature of the vapour) through measurements and simulations. Lam and Plotog worked with simple thermal profiling [15] and thermo-vision camera [16] to describe the temperature distribution inside the VPS tank. Vapour saturation and condensed droplet formation were also examined with floating polymer pillows and by optical probes [6].

In our previous studies we have examined and modeled the vapour space saturation [17] and the condensation process [18]. During these studies the Galden layer was considered to be static with a given 250 µm thickness and without any motion and convection effect in the layer. According to the optical investigations of the VPS process by Illyefalvi-Vitéz et. al [8], the concept of static condensate layer is not enough accurate approximation. During the VPS process the flow of Galden liquid is observable with changing velocity on the top side of the soldered PCB. The concept of constantly varying condensate layer is also supported by the results of highly changing vapour concentration during the VPS process which has a high impact on condensation [18]. However, in the literature of the VPS method there is no example where the dynamic changes of the condensate layer is examined. Therefore in this research we have concentrated to the dynamics of the condensate layer, such as the formation of the layer, the motion of the layer and the convective temperature transport effects. During this study the simple VPS process was investigated without soft vapour or vacuum application, in order to study how the dynamic changes of the condensate layer influence the heating efficiency and homogeneity of the VPS process.

2. Condensate layer formation model

This condensate layer formation model extends our previous board level condensation model which calculates the condensate mass on the surface of the soldered PCB according to the present values of vapour concentration and temperature (presented in [17, 18]). In this study we have concentrated only to the physics of the condensate layer.

While the basic position of the PCB during the VPS process is horizontal, the concept of the condensate layer formation is the following: at the beginning of the process condensation starts on both sides of the PCB. For the top side we can apply the most advanced Bejan model [19] (for upward facing plate with free edges), which supposes zero condensate layer height with zero hydrostatic pressure at the top edges of the plate. This causes pressure differences in the condensate layer which triggers the motion of the Galden liquid towards the edges of the plate.
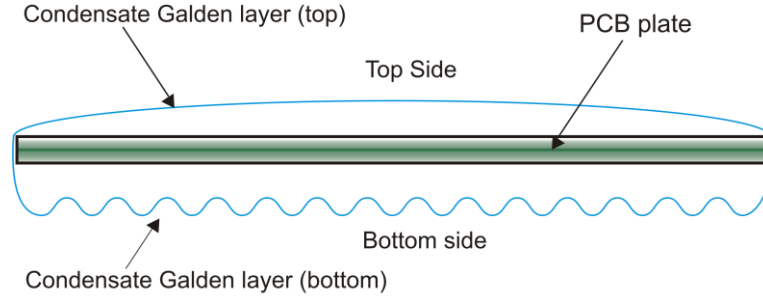
Fig. 1. Condensate layer model for a printed circuit board.

Due to the surface tension the Galden liquid flows from the upside to the down side of the plate. Dropping of the Gladen liquid does not occur until the force from the surface tension can hold the weight of the condensate. The down-flowing Galden liquid causes hydrostatic pressure difference at the bottom edges of the plate which induces movement of the layer. According to Gerstmann and Griffith, this results in a "wavy structure" of the condensate layer on the bottom side of the plate [20]. A schematic of the condensate layer model can be seen in Fig. 1.

2.1 Pysicsal description of the condensate layer formation

The governing equations of the condensate layer are given below. The continuity equation for incompressible fluids can be used since the pressure change has no effect on the density:

$$\frac{\partial v_x}{\partial x} + \frac{\partial v_y}{\partial y} + \frac{\partial v_z}{\partial z} = 0 \tag{1}$$

The Navier-Stokes equation for incompressible fluids is adopted here to close governing equations:

$$\frac{\partial v_x}{\partial t} = g_x - \frac{1}{\rho_l}\frac{\partial p_h}{\partial x} + \upsilon\left(\frac{\partial^2 v_x}{\partial x^2} + \frac{\partial^2 v_x}{\partial y^2} + \frac{\partial^2 v_x}{\partial z^2}\right) - \left(v_x\frac{\partial v_x}{\partial x} + v_y\frac{\partial v_x}{\partial y} + v_z\frac{\partial v_x}{\partial z}\right) \tag{2}$$

where v is the velocity [m/s], υ is the kinematic viscosity [m^2/s] of the Galden liquid, P_h is the hydrostatic pressure [Pa], ρ_l is the densities of the Galden liquid [kg/m^3] and g is the gravity acceleration [m/s^2]. Equation (2) can be expressed in the same way for the y and z directions. Due to the motion of the condensate layer the simple heat equation applied in the condensation model [17, 18] has to supplement with the convective parts:

$$\frac{\partial T}{\partial t} = \frac{\lambda}{\rho_l C_s}\left(\frac{\partial^2 T}{\partial x^2} + \frac{\partial^2 T}{\partial y^2} + \frac{\partial^2 T}{\partial z^2}\right) - \left(v_x\frac{\partial T}{\partial x} + v_y\frac{\partial T}{\partial y} + v_z\frac{\partial T}{\partial z}\right) \tag{3}$$

where T is the temperature [ºC], λ is the specific heat conductivity [W/m.K] and C_S is the specific heat capacity [J/kg.K].

The hydrostatic pressure in the condensate layer – what induces the movement of the Galden liquid – is calculated [19]:

$$p_h = (\rho_l - \rho_v) \cdot h \cdot g \tag{4}$$

where ρ_v is the densities of the vapour [kg/m³] and h is the height of the condensate layer [m]. The motion of the condensate layer causes a mass flow in the condensate layer which is calculated:

$$q_m = \int_A \rho_l \cdot \bar{v} \cdot dA \tag{5}$$

where q_m is the mass flow [kg/s].

During the observed VPS process the temperature change of the condensate layer is over 100ºC. Therefore the density and the kinematic viscosity of the Galden liquid cannot be considered to be constant; they are calculated according to the Galden supplier's data [21]:

$$\rho_l(T) = 1820 - 2.133 \cdot T \tag{6}$$

$$\upsilon(T) = 10^{-6} \cdot \left(0.15 + 5.655 \cdot e^{-T/31.67}\right) \tag{7}$$

The height of the condensate layer depends on the density:

$$h(T) = m / (A \cdot \rho_l(T)) \tag{8}$$

where m is the mass of the condensate [kg] and A is the area [m²] whereon the condensate height is calculated.

According to the principle of minimum energy [22], the maximum condensate thickness on the bottom side can be calculated [20]:

$$h_{\max} = \left(\sigma / (\cos\theta \cdot g_z \cdot (\rho_l - \rho_v))\right)^{0.5} \tag{9}$$

where σ is the surface tension [N/m] and θ is the decline angel of the board [rad] which is zero in our case. In this application h_{max} is ~1.05 mm, what means that the dropping of the condensate layer starts over this condensate thickness. The amount of dropping condensate depends on the spatial hydrostatic pressure gradient of the condensate layer since the condensate layer thrives for the surface with the minimum energy (so it approaches to decrease the spatial hydrostatic pressure differences). Therefore the condensate layer thickness decrease caused by the dropping is calculated (with application of Eq. 4 and 8):

$$\frac{\partial \bar{h}}{\partial \bar{r}} = \frac{1}{\rho_l \cdot g_z} \cdot \frac{\partial \bar{p_h}}{\partial \bar{r}} \tag{10}$$

where $\bar{r}$ is the local vector. It has to be noted that the goal is to approximate the thickness of the condensate layer on the bottom side – which is an important factor of the heating – and not to investigate the accurate dropping phenomenon or drop formation.

2.2 Numerical calculations

The model was implemented in MATLAB V.10 software. The model was solved by the Finite Difference Method (FDM) with the three dimensional explicit Forward Time Central Space (FTCS) algorithm. The governing equations of velocity (Eq. 2) have the following form:

$$\Delta v_{x(n)} = g_x - \left[r_{x1}\left(p_{h(n+1)}(t) - p_{h(n-1)}(t) \right) \right] + \sum_{i=x;y;z} -2r_{i,2} \cdot v_{x(n)}(t) + r_{i,2}\left(v_{x(n+1)}(t) + v_{x(n-1)}(t) \right) -$$

$$- \sum_{i=x;y;z} v_{i,(n)}(t) \left[r_{i,3}\left(v_{x(n+1)}(t) - v_{x(n-1)}(t) \right) \right] \tag{11}$$

where the coefficients are the followings:

$$r_{x1} = \frac{1}{\rho_l}\frac{\Delta t}{2\Delta x}, \quad r_{x2} = \upsilon\frac{\Delta t}{\Delta x^2}, \quad r_{x3} = \frac{\Delta t}{2\Delta x}, \quad r_{y1} = \frac{1}{\rho_l}\frac{\Delta t}{2\Delta y} \quad \ldots \tag{12}$$

where, n is the indexing of the mesh, Δt is the time step [s] and $\Delta x, \Delta y, \Delta z$ is the mesh size [m]. The other coefficient and equations towards the different directions can be produced in the same way. The governing equations of temperature (Eq. 3) have the following form:

$$\Delta T_{(n)} = \sum_{i=x;y;z} -2r_{i,1} \cdot T_{(n)}(t) + r_{i,1}\left(T_{(n+1),i}(t) + T_{(n-1),i}(t) \right) - \sum_{i=x;y;z} v_{i,(n)}(t) \left[r_{i,2}\left(T_{(n+1),i}(t) - T_{(n-1),i}(t) \right) \right] \tag{13}$$

where the coefficients are the followings:

$$r_{x1} = \frac{\lambda}{\rho \cdot C_S}\frac{\Delta t}{\Delta x^2}, \quad r_{x2} = \frac{\Delta t}{2\Delta x}, \quad r_{y1} = \frac{\lambda}{\rho \cdot C_S}\frac{\Delta t}{\Delta y^2} \quad \ldots \tag{14}$$

According to Eq. 5, the movement of the condensate layer causes mass change in the given cell:

$$\Delta m_{f(n)} = \sum_{i=x,y,z} \rho_{l(n)} \cdot \left(v_{i,(n+1)} - v_{i,(n-1)} \right) \cdot A_{i,(n)} \cdot \Delta t \tag{15}$$

According to Eq. 10, the condensate thickness change on the bottom side caused by the dropping is calculated:

$$\Delta h_{(n)} = \sum_{i=\pm x,\pm y} \frac{1}{\rho_{l(n)} \cdot g_z} \cdot \left(p_{h(n+i)} - p_{h(n)} \right) \tag{16}$$

The mass change caused by the dropping effect is calculated by Eq. 6 and 8:

$$\Delta m_{d(n)} = A \cdot \rho_{l(n)} \cdot \Delta h_{(n)} \tag{17}$$

According to Eq. 4, 6, 8 and 10 the mass change results in the change of the hydrostatic pressure in the given cell:

$$\Delta p_{h(n)} \cong \frac{\left(\Delta m_{f(n)} + \Delta m_{d(n)} \right) \cdot g_z}{\Delta x \cdot \Delta y} \tag{18}$$

where the hydrostatic effect of the Galden vapour is neglected, since the density of the Galden liquid 2 order of magnitude higher than the density of the Galden vapour.

The initial temperature for the board is $T(0)=40$ ºC (due to the moderate preheating effect of the VPS tank before the immersion of the PCB into the vapour). The initial conditions for the condensate layer is $v(0)=0$ m/s, $p_h=0$ Pa and $m(0)=0$ kg (it does not exist before the immersion). The initial condition of the vapour space is defined by the pre-calculation of the process model [17, 18]. The border conditions of the condensate layers for the top side are the followings [19]:

$$\frac{\partial T}{\partial r} = 0 \; ; \; \lim_{r \to bord.} p_h = 0 \; ; \; \lim_{r \to bord.} v = \infty \tag{19}$$

and for the bottom side:

$$\frac{\partial T}{\partial r} = 0 \; ; \; v\big|_{r=bord.} = 0 \tag{20}$$

3. Experimental procedures and Model discretisation

A batch type, experimental VPS oven was used for our investigation. The oven was constructed in our laboratory (details of development are published in [6, 9]). The base unit of the oven is a double walled (thickness is 0.5 mm) stainless steel tank with a removable lid cover. The lid has a heat-resistant glass window and an aperture for measurement probes. The tank dimensions are the following: width 180 mm (x axis); length 280 mm (y axis); height 170 mm (z axis). An immersion resistor heater (positioned 10 mm from the bottom of the tank) is applied for heating the Galden liquid which is constructed from ⌀1 mm heater filaments (~25 Ω resistance) with ceramic filler covered by a ⌀10 mm stainless steel tube. The excess vapour is condensed by a cooler appliance (positioned 10 mm under top of the tank) which is a ⌀10 mm copper tube with circulated room temperature water. In Fig. 2 the schematic of the VPS oven can be seen.
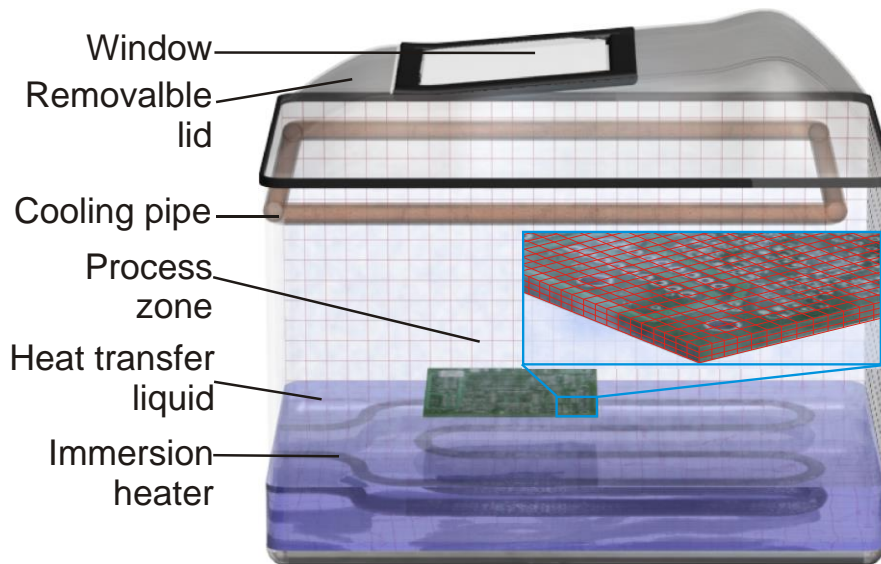
Fig. 2. The applied VPS oven with the applied numerical grid of the process and the condensate layer formation model.

HT170 type Galden with 170 °C boiling point was used for the investigations. The applied amount of Galden was 1.3 dm^3. The relatively low boiling point (compared to the conventional lead-free soldering temperatures at 245 °C.) was chosen in order to get validation results faster in time; since during the verification measurements the heating and cooling cycles of the system are much shorter in this case. A full heating-cooling cycle is still around ~3 hours which is very long compared to the ~30 sec soldering time. In addition, HT170 is also relevant from the aspect of low melting point solder alloys such as Sn-Bi types. The applied heating and cooling power was 550W and 50W, respectively.

The condensate layer formation was studied on the surface of a simple FR4 panel with 80x80x1.5 mm^3 size. The simulated test board was divided into 40x40x3 cells (along the *x, y, z* axes respectively), covered by 1−1 condensate layer at top- and bottom side and 1−1 further vapour cell-layer. Cuboid cells were applied in a uniform grid with: 2x2x0.5 mm sizes (along the *x, y, z* axes respectively), except the condensate layer where dynamic thickness was applied. In this partition the model has 11200 cells altogether. The model contains the following types of cells: FR4 panel, Galden liquid and Galden vapour cells. The parameters of the used materials can be seen in Tab. 1.

Tab. 1. Physical parameters of applied materials.

	Density [kg/m^3]	Spec. heat cap. [J/kg.K]	Spec. therm. cond. [W/m.K]	Latent heat [J/kg]
Galden liq.	1820	973	0.07	67000
Galden vp.	20*	973	0.07	67000
FR4	2100	570	0.25 $^{(x,y)}$; 0.17 $^{(z)}$	-

* Saturation vapour concentration at 170°C.

As it was discussed in the Introduction section the condensate layer formation model is an extension of our board level condensation model [18] which has an embedded structure and runs together with the process level model of VPS (presented in [17]). The process model supplies the vapour space parameters in each step for the Galden layer formation model and vice versa. This means that in each calculation step, the condensation model does a resolution refinement in those cells of the process model wherein it is located and after the calculations it reorders the cells with the modified values for the next step of the process model. (The exact algorithm is presented in [18]). The main advantage of the embedded construction is that the process model can work with much lower resolution ($10 \times 10 \times 10$ mm^3) than the Galden layer formation model which ensures much faster operation for the system. The applied grid of the process and the condensate layer formation model can be seen in Fig. 2. The stability and the convergence criterion of applied numerical method (FTCS) is: $r_x + r_y + r_z \leq 0.5$. The stability and convergence analysis results in that $\Delta t < 0.008$ s (in the case of the applied grid). In order to reduce the truncation error, the time step is reduced to $\Delta t = 0.005$ s.

Unfortunately accurate optical measurement cannot be carried out for verification of the condensate layer formation since the layer is diffuse but the vapour space is not. The spontaneous "Galden rain" [8] due to the condensation around the top lid and the particles in the vapour space would also disturb the optical investigations. In addition the maximum thickness of the condensate layer is ~200 µm. The Galden is inert; therefore some kind of level measurement through chemical reagents is also impossible. However the thickness of the condensate layer changes the thermal diffusivity of the layer. Therefore the condensate layer formation can be verified via temperature change measurements of the heated test board. The temperature measurements were performed with K-type thermocouples (absolute measurement accuracy was ±0.5 °C) at different locations inside the board (the thermocouples were embedded into the board to avoid the perturbation of the condensate layer formation).

The verification of the condensate layer formation model has started after 16 minutes preheating of the VPS system. Results of the verification can be seen in Fig. 3 where the pervious verification results of the simple condensation model [18] – which applies static condensate thickness – is also presented. It can be concluded that the match of the results with the dynamic condensate layer (red curves) is better than in the case of the static condensate layer (blue dashed curve). In addition, the model with the static condensate layer has produced the same calculation results at any location of the board. Therefore the simulation results become more accurate with the modeling of the condensate layer formation. The absolute error decreased from 5% under 1%.
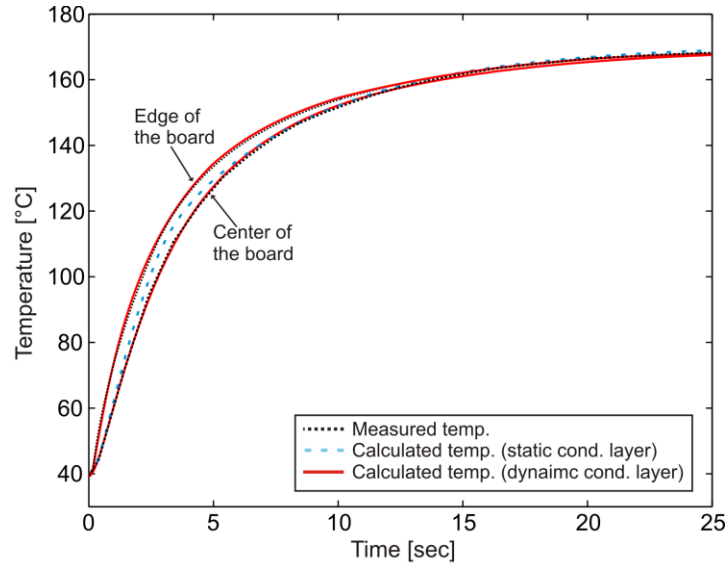
Fig. 3. Verification results.

4. Results

The results of the condensate layer formation were analyzed separately on the top and bottom side of the board. On the further condensate layer visualizations the following parameters are presented: the thickness, the temperature and the *x-y* projection of the velocity vectors. Different scaling of the axes was applied due to the better visualization of the layer thickness; however it causes a minor visual distortion in the representation. The presented surfaces are truncated at edges of the PWB due to the visualization of the velocity vectors. The velocity vectors represent the direction of the flow and the relative velocity differences. (Detailed discussion of the absolute velocity values will be presented later.)

According to the results on the top side (Fig. 4), the condensation is very intense after the immersion of the board into the vapour space. At 0.5 s the thickness of the condensate reaches 100 µm (Fig. 4a). The fast thickness increase results in high hydrostatic pressure gradients at the edges which cause sudden velocity increase of the condensate towards the edges (Fig 4a-b). This effect results in that the thickness of the condensate layer decreases at the edges very soon (Fig. 4b)). A slight corner effect is also observable both on the temperature and the thickness values. Between 1.5 – 2 s the condensate thickness reaches the maximum value over 200 µm (Fig. 4c), then the layer thickness is decreasing, since the condensing mass is less than the mass of the down-flowing liquid.
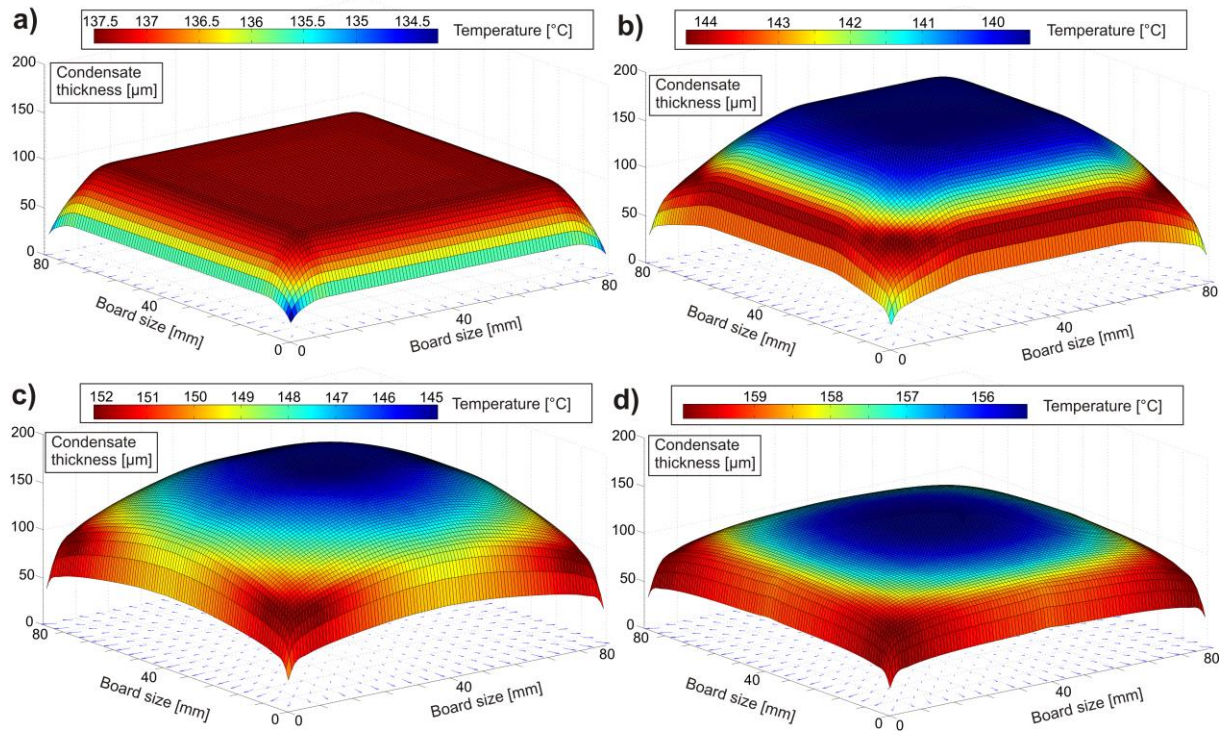
Fig. 4. Condensate layer on the top side, a) at 0.5 s; b) at 1 s; c) at 2 s; d) 4 s.

However the decrease of the layer is not as fast as the increase since the flow velocity is decreased by the convective component (in Eq. 2.) and there is still condensation up to ~4 s (Fig 4d)) where the temperature reaches the dew point in the whole layer (the region at the edges reaches the dew point a bit faster).

In Fig. 5 the condensate thicknesses, the absolute flow velocities, the temperature differences and the mass flows are analyzed on the top side of the board from the center towards a corner (red curves) and towards a side (blue curves) during the whole soldering process. The effect of rapid velocity increase between 0 –1.5 sec (Fig. 5b) results in break points on the condensate thickness curves (Fig. 5a) at the starts of the high gradient velocity increase periods. The thickness increase is slowing (or sometimes changes to decrease) when the velocity increase starts.
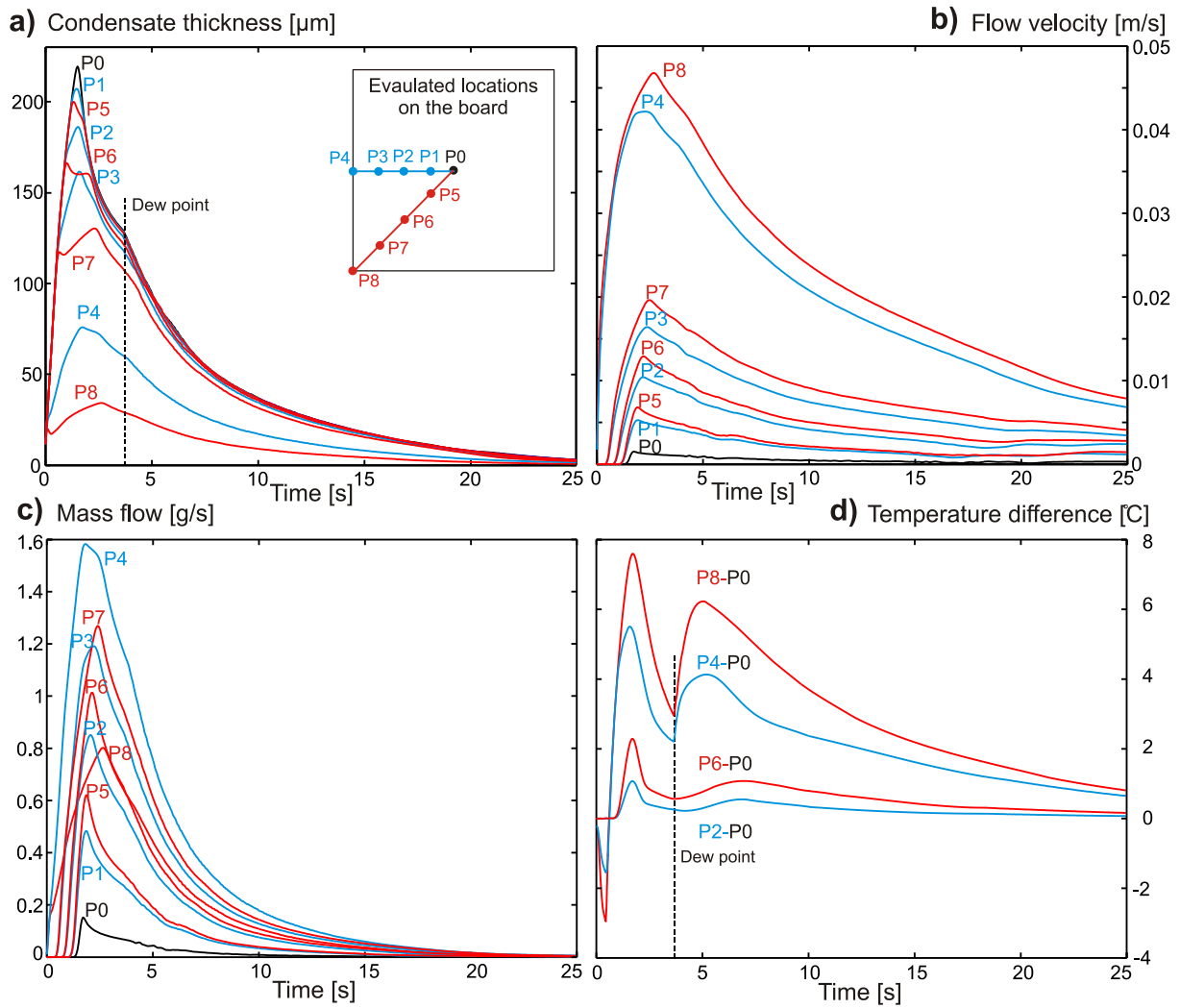
Fig. 5. Condensate layer parameters during 25 s time period on the top side, a) condensate thickness, b) flow velocity, c) mass flow, d) temperature difference compared to the center.

The previously discussed dew point – where the condensation is stopped – is also visible in Fig. 5a which makes the thickness decrease faster. At the end of the process (25 sec) the condensate layer thickness decreases under 10 µm (Fig. 5a). The flow velocity (Fig. 5b) and the mass flow (Fig. 5c) is more intense towards the corners than the sides, however at the corners the very low layer thicknesses cause much lower mas flow values (P8) compared to the sides (P4).

As it was visible in Fig. 4, considerable temperature differences are formed in the condensate layer on the top side. Between 0 – 0.5 sec, before the high gradient velocity increases (Fig. 5b) the condensate layer is colder at the edges (Fig. 5c and Fig. 4a) since the thinner condensate at the edges has smaller heat capacity and cold down faster as the thicker condensate towards the center. Between 0.5 – 1.5 sec when the flow velocities have the maximum values, the previous trend reverses due to the convection effect (Eq. 3) and the maximum temperature difference reaches +7.8 ºC (Fig. 5c). Between 1.5 – 4 sec when the flow

velocity decreases, the temperature differences also have a monotone decrease, however remains over zero during the whole process. The stop of the condensation (after the dew point) perturbs the temperature distribution in the condensate layer. Between 4 – 6 sec the temperature differences starts to increase again since the "extra" energy of the condensation for the center region is disappeared (as it was discussed the dew point is reached faster at the edges, around ~3 sec).   After 6 sec when the previous effect vanished, the temperature differences starts to decrease again. The fluctuating temperature distribution also influents the heating of the soldered PCB; this phenomenon will be discussed later.

Fig. 6 presents the condensate layer on the bottom side where the zero level is at the bottom of the board. Besides the intense condensation, the down-flowing condensate form the top side also accumulates on the bottom side of the board. This causes fast thickness increase, at 1 s the condensate thickness reaches ~200 μm. The continuously down-flowing Galden from the top perturbs the bottom layer which forms a wavy structure (Fig. 6).
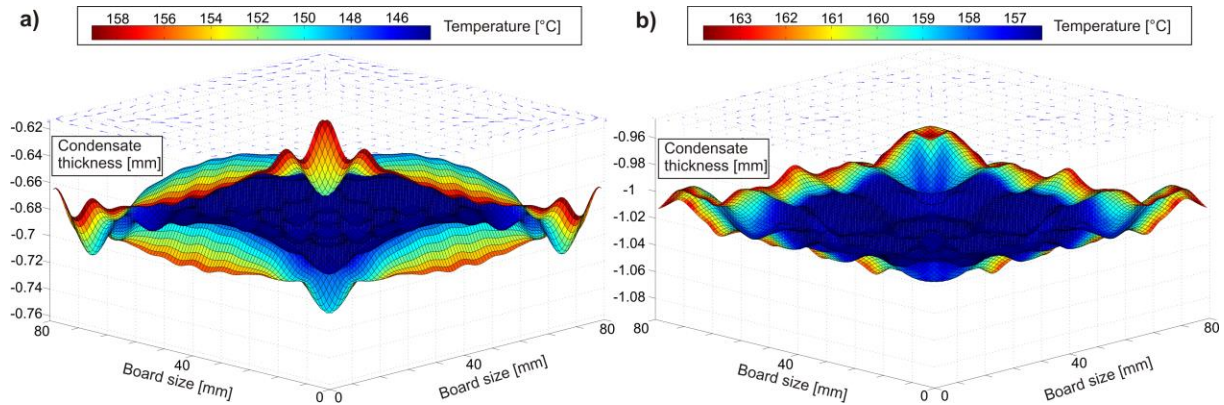

Fig. 6. Condensate layer on the bottom side, a) at 4 s; b) at 11s.

Around ~11 sec, at specific points of the wavy layer the thickness reaches the maximum value (h_{max} = ~1.05 mm) where the dropping starts (Fig. 6b). After this point the increase of the layer thickness has stopped and it starts to equalize around 1.05 mm level. The down-flowing Galden from the top side and the dropping results in disordered flow field on the bottom side without dominant flow direction.

In fig. 7 the condensate parameter analysis can be seen on the bottom side. The maximum thickness differences are between 10 – 15% in the first 11 sec, after the start of the dropping it decreases to 1 – 2% (Fig. 7a). As it was previously discussed the flow field is disordered on the bottom side (Fig. 7b) and the maximum velocity values are 15 times smaller compared to the top side (Fig. 5b). It is also visible in the flow analysis of the bottom side (Fig. 7b-c), that the condensation starts again for short times after the "global" dew point at 4 sec. This is also barely visible on the results of the top side as minor velocity increases (Fig. 5b). The mass flow

differences towards the different directions are also smaller on the bottom side compared to the velocity differences.
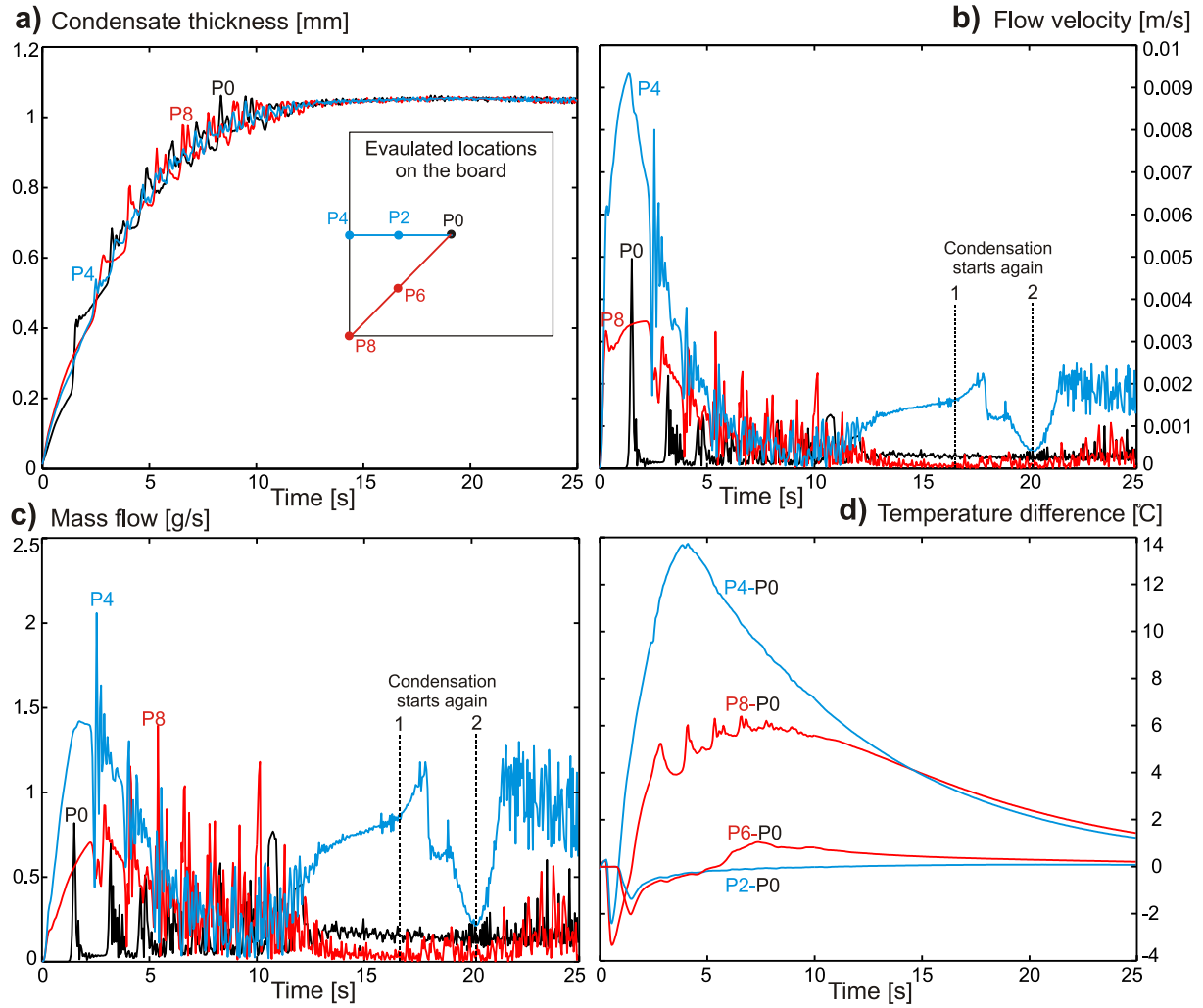

Fig. 7. Condensate layer parameters during 25s time period on the bottom side, a) condensate thickness, b) flow velocity, c) mass flow, d) temperature difference compared to the center.

Even though much smaller velocities are observable on the bottom side, the mass flow values are in the same order of magnitude with the values on the top side (Fig. 5c and 7c). This phenomenon is due to the 10 times thicker condensate layer on the bottom side.

   The temperature distribution is more homogeneous on most of the bottom surface expect at the edges where the maximum temperature difference reaches +13.8 ℃ which is the double of the top side results (Fig. 6a-b and 7d). This interesting situation is caused by the combined effect of the relatively equal condensate thickness, the huge amount of down-flowing Galden liquid from the top edges to the bottom edges and the temperature difference between the condensate layers. (The thinner condensate layer on the top side is warmer due to its smaller heat capacity as it is visible when compare Fig. 4d and 6b.). Between $0-4$ sec the temperature changes at the bottom edges show similar behavior with the top side results. Between $4-6$ sec

the effect of the dew point is not visible here due to the much higher heat capacity of the thick condensate layer on the bottom side.

The previously discussed effects can cause heating ability differences during the VPS process which is presented in Fig. 8. The temperature differences on the surface of the soldered board are smaller (Fig. 8a-b) as in the condensate layer (Fig. 5d and 7d), this is observable mainly in the case of the bottom side of the board. However the maximums can reach 7 ºC at the edges of the board (P4 and P8). Therefore it is suggested to optimize keepout regions for the components at the edges of the PCB during the design of the circuit if it will be assembled by VPS. From P3 and P7 points towards the center of the board (what covers ~75% area of the board) the temperature difference is under 3 ºC what is outstanding in the field of reflow soldering technologies. According to the thermal profile analysis (Fig. 8c), the heating up of the bottom side is not as rapid as it is on the top side. This is caused by the ~10 times bigger heat capacity of the condensate layer on the bottom side compared to the top side. Around 5 sec after the immersion, for a while the maximum differences can reach 14 ºC between the same points on the top and bottom side. This effect alone cannot cause soldering failures; however it is suggested to fit the process time to the demands of the bottom side during the setting of the soldering parameters.
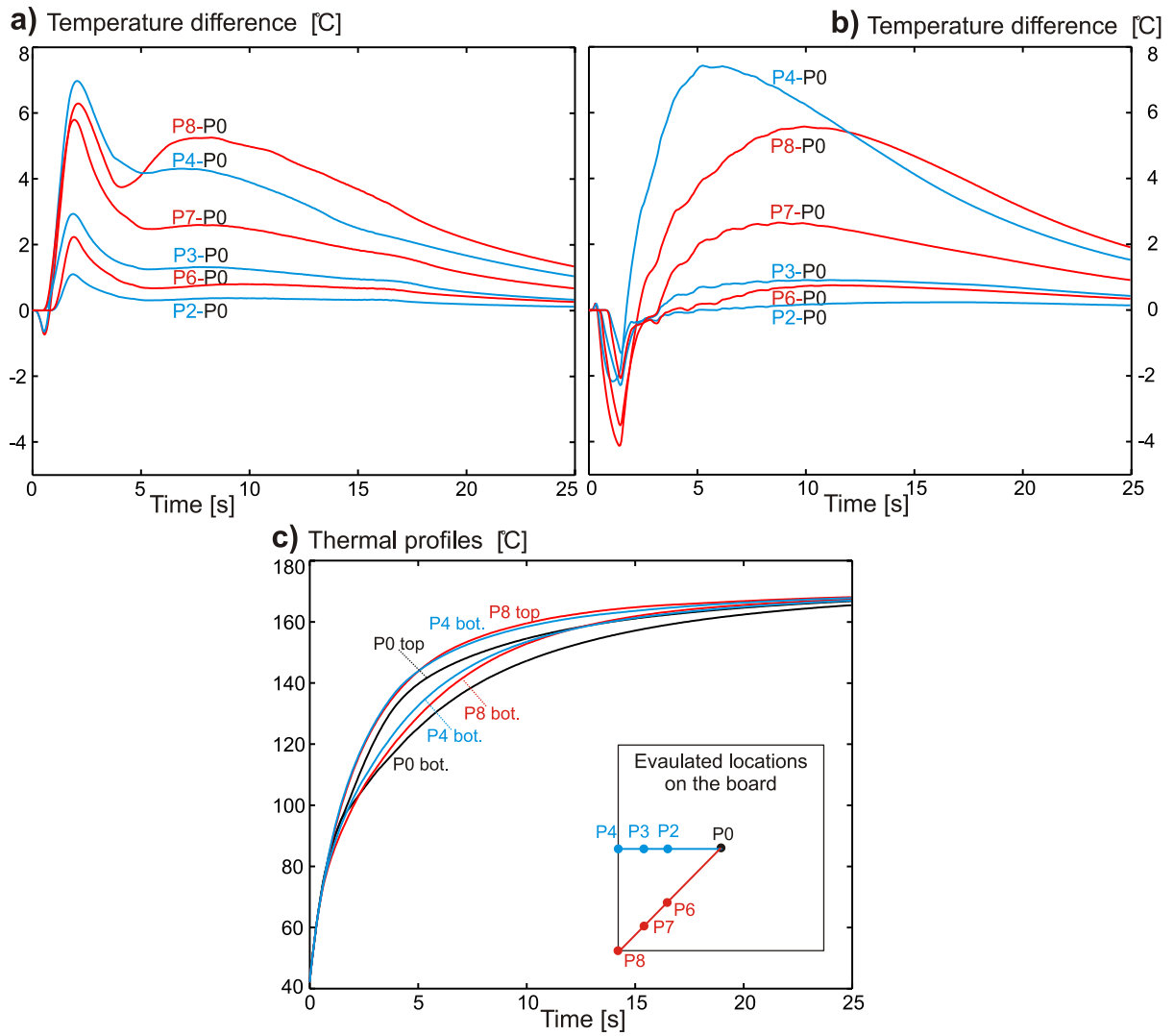
Fig. 8. Temperature analysis of the soldered board, a) temperature differences on the top side, b) temperature differences on the bottom side, c) thermal profiles on the top and bottom side.

5. Conclusions

A modeling approach of the Galden layer formation on the surface of the soldered board during the VPS process was presented. It was shown that the numerical modeling of the VPS process becomes more accurate with application of dynamic condensate layer instead of a static description. It was found that, the condensation is very intense after the immersion of the board into the saturated vapour space. On the top side the change of the condensate is very dynamic, the layer thickness reaches the maximum value (0.2 mm) around 1.5 s and then it starts to decrease. The thickness decrease is slower than the thickness increase. The maximum flow velocity (0.048 m/s) is observed around 2 s at the corners of the board while the maximum mass flow (1.59 g/s) is found at the sides (in the same time). On the bottom side the intense condensation and the down-flowing condensate from the top side causes a fast and continuously increasing condensate thickness, until ~11 sec when the thickness reaches the

maximum value (1.05 mm) and the dropping starts. The down-flowing Galden from the top side and the dropping results in wavy shape of the condensate and disordered flow filed on the bottom side without dominant flow direction.

Due to the down-flowing condensate, the temperature increases towards the edges of the board (also on the top and bottom side) which result in higher heating gradient at the edges. The maximum temperature difference can reach 7 ºC between the edges and the center of the board. Therefore it is suggested to intentionally design component keepout regions at edges during the design of the circuit if it will be assembled by VPS. On the other ~75% area of the board the temperature difference is under 3 ºC what is acceptable. The heating up of the bottom side is not as rapid as it is on the top side due to the ~10 times higher amount of the condensate on the bottom side. This effect is not able to cause soldering failures in itself; however it is suggested to fit the process time to the demands of the bottom side during the setting of the soldering parameters.

Acknowledgment

References

[1] M. Bassi, Estimation of the vapor pressure of PFPEs by TGA, Thermochim. Acta. 521 (2011) 197– 201.

[2] H. Benli, A performance comparison between a horizontal source and a vertical source heat pump systems for a greenhouse heating in the mild climate Elazig, Turkey, App. Therm. Eng. 50 (2013) 197-206.

[3] Y. Li, H. He, Z. Zeng, Evaporation and condensation heat transfer in a heat pipe with a sintered-grooved composite wick, App. Therm. Eng. 50 (2013) 342-351.

[4] X. Liu, Y. Xiao, K. Inthavong, J. Tu, A fast and simple numerical model for a deeply buried underground tunnel in heating and cooling applications, App. Therm. Eng. 62 (2014) 545-552.

[5] M. Ge, J. Zhao, S. Wang, Experimental investigation of steam condensation with high concentration CO_2 on a horizontal tube, App. Therm. Eng. 61 (2013) 334-343.

[6] A. Géczy, Zs. Illyefalvi-Vitéz, P. Szőke, Investigations on Vapor Phase Soldering Process in an Experimental Soldering Station, Micro and Nanosyst. 2 (2010) 170-177.

[7] O Krammer, T. Garami, Comparing the intermetallic layer formation of Infrared and Vapour Phase soldering, in Proceed. of 34th IEEE-ISSE conf., Tatranska Lomnica, Szlovakia, 2010, pp. 196-201.

[8] Zs. Illyefalvi-Vitéz, A. Géczy, R. Bátorfi, P. Szőke, Analysis of Vapor Phase Soldering in Comparison with Conventional Soldering Technologies, in Proceed. of 3rd IEEE-ESTC conf., Berlin, Germany, 2010, paper No. 0283.

[9] A. Géczy, Zs. Péter, Zsolt, Zs. Illyefalvi-Vitéz, 3D Thermal Profiling of an Experimental Vapour Phase Soldering Station, in Proceed. of 34th IEEE-ISSE conf., Tatranska Lomnica, Szlovakia, 2011, pp. 89-93.

[10] O. Krammer, T. Garami, Investigating the Mechanical Strength of Vapor Phase Soldered Chip Components Joints, in Proceed. of IEEE Int. Symp. for Design and Techn. in Electron. Pack., Pitesti, Romania, 2010, pp. 103-106.

[11] J.Villain, M. Beschomer, H.J. Hacke, B. Brabetz, J. Zapf, Formation, Distribution and Failure Effects of Voids in Vapor-Phase Soldered Small Solder Volumes, in Prceed. of IEEE Int. Symp. on Adv. Pack. Mater, Braselton, USA, 2000, pp. 141-144.

[12] G. M. Freedman, Soldering Techniques, Vapor-Phase Reflow Soldering, in (Ed.) C. F. Coombs, Jr., Printed Circuits Handbook, 6th ed., McGraw-Hill, New York, USA, 2008, pp. 47/42-43.

[13] C. Zabel, A. Duck, Vapour phase vacuum-soldering. A new process technology opens tremendous production capabilities when reflow-soldering, in Proceed. of Intern. Conf. Solder. Reliab., Toronto, Canada, 2009, paper No. 6.

[14] H. Leicht, A. Thumm, Today's Vapor Phase Soldering - An Optimized Reflow Technology for Lead Free Soldering, in Proceed. of Surf. Mount Tech. Assoc. Intern. Conf., Orlando, USA, 2008, paper No. 45.

[15] I. Plotog, T. Cueu, B. Mihaileseu, G. Varzaru, P. Svasta, I. Busu, PCBs with Different Core Materials Assembling in Vapor Phase Soldering Technology, in Proceed. of 9th ISETC conf., 2010. pp. 421-424.

[16] D.M. Lam, Vapour Phase Soldering Device, PhD Thesis, Czech Technical University In Prague, 2011.

[17] B. Illés, A. Géczy, Multi-Physics Modelling of a Vapour Phase Soldering (VPS) System, App. Therm. Eng. 48 (2012) 54-62.

[18] B. Illés, A. Géczy, Investigating the dynamic changes of the vapour concentration in a Vapour Phase Soldering oven by simplified condensation modelling, App. Therm. Eng. 59 (2013) 94-100.

[19] A. Bejan, Film condensation on an upward facing plate with free edges, Int. J. Heat Mass Transf. 34/2 (1991) 582-587.

[20] J. Gerstmann, P. Griffith, Laminar film condensation on the underside of horizontal and inclined surfaces, Int. J. Heat Mass Transf. 10 (1966) 567-580.

[21] Daitoku Tech, Co., LTD., Manufacturer datasheet of Galden fluid, http://www.daitokutech.com/products/galden/data/HT170.pdf

[22] O. Krammer, Modelling the Self-Alignment of Passive Chip Components during Reflow Soldering, Microelectron. Reliab., in Press, DOI: 10.1016/j.microrel.2013.10.010.

Figures and Tables:

Fig. 1. Condensate layer model for a printed circuit board.

Fig. 2. The applied VPS oven with the applied numerical grid of the process and the condensate layer formation model.

Fig. 3. Verification results.

Fig. 4. Condensate layer on the top side, a) at 0.5 s; b) at 1 s; c) at 2 s; d) 4 s.

   Fig. 5. Condensate layer parameters during 25 s time period on the top side, a) condensate thickness, b) flow velocity, c) mass flow, d) temperature difference compared to the center.

Fig. 6. Condensate layer on the bottom side, a) at 4 s; b) at 11s.

 Fig. 7. Condensate layer parameters during 25s time period on the bottom side, a) condensate thickness, b) flow velocity, c) mass flow, d) temperature difference compared to the center.

 Fig. 8. Temperature analysis of the soldered board, a) temperature differences on the top side, b) temperature differences on the bottom side, c) thermal profiles on the top and bottom side.

Tab. 1. Physical parameters of applied materials.

	Density [kg/m^3]	Spec. heat cap. [J/kg.K]	Spec. therm. cond. [W/m.K]	Latent heat [J/kg]
Galden liq.	1820	973	0.07	67000
Galden vp.	20*	973	0.07	67000
FR4	2100	570	0.25 $^{(x,y)}$; 0.17 $^{(z)}$	-

* Saturation vapour concentration at 170°C.